

Scattering singularity in topological dielectric photonic crystals

Langlang Xiong^{1,4}, Xunya Jiang^{1,2,3,*} and Guangwei Hu^{4,†}

¹*Institute of Future Lighting, Academy for Engineering and Technology, Fudan University, Shanghai 200433, China*

²*Department of Illuminating Engineering and Light Sources, School of Information Science and Engineering, Fudan University, Shanghai 200433, China*

³*Engineering Research Center of Advanced Lighting Technology, Fudan University, Ministry of Education, Shanghai 200433, China*

⁴*School of Electrical and Electronic Engineering, 50 Nanyang Avenue, Nanyang Technological University, Singapore 639798, Singapore*



(Received 27 March 2024; revised 5 June 2024; accepted 6 June 2024; published 26 June 2024)

The exploration of topology in natural materials and metamaterials has garnered significant attention. Notably, the one-dimensional (1D) and two-dimensional (2D) Su-Schrieffer-Heeger (SSH) models, assessed through tight-binding approximations, have been extensively investigated in both quantum and classical systems, encompassing general and higher-order topology. Despite these advancements, a comprehensive examination of these models from the perspective of wave physics, particularly the scattering view, remains underexplored. In this study, we systematically unveil the origin of the 1D and 2D Zak phases stemming from the zero-reflection point, termed the scattering singularity in momentum space. Employing an expanded plane wave expansion, we accurately compute the reflective spectrum of an infinite 2D photonic crystal (2D-PhC). Analyzing the reflective spectrum reveals the presence of a zero-reflection line in the 2D-PhC, considered the topological origin of the nontrivial Zak phase. Two distinct models, representing omnidirectional nontrivial cases and directional nontrivial cases, are employed to substantiate these findings. Our work introduces a perspective for characterizing the nature of nontrivial topological phases. The identification of the zero-reflection line not only enhances our understanding of the underlying physics but also provides valuable insights for the design of innovative devices.

DOI: [10.1103/PhysRevB.109.224111](https://doi.org/10.1103/PhysRevB.109.224111)

I. INTRODUCTION

The exploration of topological phenomena in quantum and classical systems [1–11] has garnered widespread interest due to their ability to host robust states, exemplified by edge states [12–17] and corner states [18–20]. In the realm of topology, a classic analogy depicts a donut or a coffee mug, both possessing one hole, as homeomorphic, categorizing this as nontriviality. In contrast, a holeless cow and a sphere, both lacking holes, are deemed trivial [21]. The band topology of an isolated band in quantum and classical systems can be likened to finding a “hole” in a band. For a nontrivial band, discernible topological invariants such as the Zak phase [22,23] or Chern number [24–26] can be identified. Most topological systems explored thus far have originated from tight-binding models, notably the one-dimensional (1D) and two-dimensional (2D) Su-Schrieffer-Heeger (SSH) model [15,23,27]. Whether in the context of 1D or 2D SSH models, the manipulation of topological phases is readily achievable by adjusting intracell and intercell coupling strengths. This simplicity, facilitated by a straightforward Hamiltonian, enables the comprehensive calculation of topological properties.

However, classical wave systems, such as photonic systems, present a unique challenge due to non-negligible long-range coupling dictated by Maxwell’s equations. This intricate coupling cannot be succinctly described by a simple

tight-binding Hamiltonian [28,29]. While analogous phenomena may be observed in both wave and tight-binding systems, elucidating a distinctive topological origin in wave systems poses a significant hurdle. Specifically, the question arises: can we accurately pinpoint the “hole” in a band using the classical wave method, specifically through the lens of scattering?

In this study, we first employ the transfer matrix method [30] to precisely correlate the topological scattering singularity in 1D photonic crystals (PhCs), a zero-reflection point within the reflective spectrum with the Zak phase. Subsequently, our focus shifts to 2D-PhCs. To address the challenge of calculating the scattering of a half-infinite 2D-PhC, we meticulously introduce the expanded plane wave expansion method (EPWE) [31,32]. Our analysis delves into two scenarios in 2D-PhCs. First, the two-rods square models without C_4 and $M_{x(y)}$ symmetries serve to illustrate the singularity-induced gap-closed-reopened process and topological phase transition [17]. Second, the four-rods square models with $M_{x(y)}$ symmetry showcase the singularity behavior in directional Zak phase [15]. This comprehensive approach enhances our understanding of the topological scattering singularity in 2D-PhCs. Our work introduces a perspective for considering the topological origin in classic systems, holding promise for advancing the development of new topological photonic devices.

II. SCATTERING SINGULARITY IN 1D-PHC

In this section, we will systematically define the concept of scattering singularity and elucidate its impact on band

*Contact author: jiangxunya@fudan.edu.cn

†Contact author: guangwei.hu@ntu.edu.sg

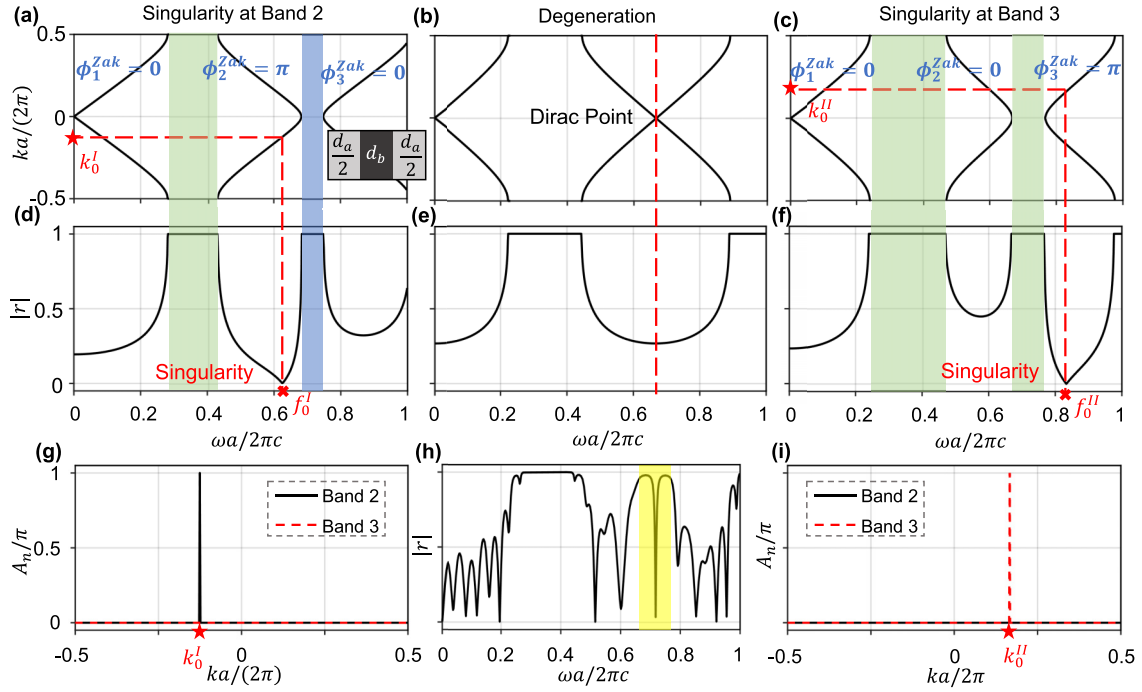


FIG. 1. Singularity-induced topological phase transition in 1D-PhC. (a), (d), and (g): Band structure, reflective spectrum, and A_n distribution, respectively, illustrating the singularity at band 2 with parameters $d_a = 0.6a$, $d_b = 0.4a$, $\varepsilon_a = 1$, $\varepsilon_b = 4$. The blue range represents the perfect magnetic conductor (PMC) gap, and the green range indicates the perfect electrical conductor (PEC) gap; (b) and (e): Band structure and reflective spectrum in the case of band degeneracy with parameters $d_a = 0.75a$, $d_b = 0.25a$, $\varepsilon_a = 1$, $\varepsilon_b = 9$; (c), (f), and (i): same as (a), (d), and (g), respectively, but showcasing the singularity at band 3 with parameters $d_a = 0.8a$, $d_b = 0.2a$, $\varepsilon_a = 1$, $\varepsilon_b = 9$; (h): Reflective spectrum of the structure formed by three layers of the model in (a) and five layers of the model in (c), with the edge state marked in the yellow range.

topology in 1D-PhC. While the most mathematical derivations are provided in the Appendix of this work [30], this section aims to focus on physical insights.

Under the transfer matrix method (TMM) gauge in a mirror-symmetric 1D-PhC with two types of materials, it can be proven that if an isolated band (excluding the first band) encompasses one resonance frequency point of the unit cell, then the Zak phase of this band must be π [30], designating such a zero-reflective resonance frequency point as a singularity from the scattering view. We should note that zero reflection only means the coherent sum of all orders of scattering is zero, not all orders of scattering are zero. For more complex cases, i.e., 1D-PhC with more than two types of materials, there may be more than one singularity in an isolated band, then the topological phase of this band is determined by the sum phases of all singularities [28,33,34], meaning the topological phase determined by singularities is a global property. Consider, for example, the simplest model of a 1D-PhC with lattice constant a , as illustrated in Fig. 1. In this model, the unit cell comprises two types of layers: layer A with relative permittivity ε_a , permeability μ_a , and thickness d_a , and layer B with relative permittivity ε_b , permeability μ_b , and thickness d_b . Such a unit cell is also known as a FabryPérot (FP) cavity, with a resonance condition defined as $\sin(k_b d_b) = 0$. Consequently, the resonance frequency is given by $f = m \cdot c / (2n_b d_b)$, where $m = 1, 2, 3, \dots$, $k_b = n_b \omega / c$ is the wave vector, $\omega = 2\pi f$ is the angular frequency, and $n_b = \sqrt{\varepsilon_b \mu_b}$ represents the refractive index of layer B.

Consequently, the position of the singularity can be specifically determined by altering the material or geometry of the cavity.

For a finite 1D-PhC comprising N cells, a band that includes the resonance frequency of the unit-cell yields N peaks. Conversely, it results in $N - 1$ peaks if the resonance frequency is not encompassed [35] (refer to the Appendix for further details). When this is extrapolated to an infinite 1D-PhC, it will be demonstrated that a band containing the resonance frequency of a single unit cell will produce one resonance peak; if it does not, no resonance peaks will be observed.

To visually observe how the singularity alters the band topology, we consider three parameter sets where the singularity moves from the lower band to the degenerate point and eventually to the upper band. In case I [Figs. 1(a) and 1(d)], the singularity resides in the lower second band with parameters $d_a = 0.6a$, $d_b = 0.4a$, $\varepsilon_a = 1$, $\varepsilon_b = 4$. In case II [Figs. 1(b) and 1(e)], the singularity is at the degenerate Dirac point between the second and third bands with parameters $d_a = 0.75a$, $d_b = 0.25a$, $\varepsilon_a = 1$, $\varepsilon_b = 9$. Finally, in case III [Figs. 1(c) and 1(f)], the singularity is at the third band with parameters $d_a = 0.8a$, $d_b = 0.2a$, $\varepsilon_a = 1$, $\varepsilon_b = 9$. Clearly, as the singularity moves, the second gap undergoes closure and reopening, a hallmark of topological phase transition. Notably, when the singularity is at the second band, the Zak phase of the second band is π , while that of the third band is zero. Conversely, when the singularity is at the third band,

the results are reversed. The nature of the second gap also changes, transitioning from a nontrivial perfect magnetic conductor (PMC)-like gap to a trivial perfect electrical conductor (PEC)-like gap. In other words, the effective medium at the gap transitions from mu negative (MNG) to epsilon negative (ENG) materials [36,37]. Consequently, combining the two photonic crystals reveals the presence of an edge state in the second gap, as illustrated in Fig. 1(h). This prompts the question: how are the scattering singularity and band topology connected? To answer this, we must revert to the definition of Zak phase for an isolated band:

$$\phi_n^{\text{Zak}} = \int_{\text{FBZ}} dk i \langle u_{n,k} | \partial_k u_{n,k} \rangle, \quad (1)$$

where $|u_{n,k_j}\rangle$ is the normalized periodic part for n th band at k_j (Bloch wave vector) of the field in a cell, and FBZ means the first Brillouin zone. The Zak phase can be numerically calculated using the Wilson loop [38]:

$$\begin{aligned} \phi_n^{\text{Zak}} &= \sum_{j \in \text{FBZ}} A_n \\ &= \sum_{j \in \text{FBZ}} -\text{Im} \left\{ \ln \left[\langle u_{n,k_j} | u_{n,k_{j+1}} \rangle \right] \right\}. \end{aligned} \quad (2)$$

It's noteworthy that the product A_n does not depend on the phase of $|u_{n,k_j}\rangle$ s. In Figs. 1(g) and 1(i), we display each A_n for the second band and third band in FBZ for case I and case III, respectively. Notably, at the point (f_0^I, k_0^I) of case I, there is a sudden change of A_n , and similarly, at the point (f_0^{II}, k_0^{II}) of case III, a sudden change is observed in the A_n . This phenomenon can be elucidated by the fact that $|u_{n,k_0^-}\rangle = -|u_{n,k_0^+}\rangle$, as shown in Fig. 2, providing an explanation for the observed phase change at the singularity [30]. Furthermore, within the context of TMM gauge, it is essential to emphasize that the group velocity at the singularity must be positive, ensuring the existence of only one singularity at a fixed frequency.

III. SCATTERING SINGULARITY IN 2D-PHC

Unlike the perfect gauge of TMM in 1D-PhC, when transitioning to 2D systems, certain challenges arise in researching the singularity. First, the challenge of finding points that fulfill $|u_{n,k_0^+}\rangle = -|u_{n,k_0^-}\rangle$ since a random phase will be introduced when calculating the eigen-function of 2D-PhC. Fortunately, this can be addressed in the calculation of the Zak phase, thanks to the gauge independence of the Wilson loop, leading to the cancellation of the random phase. What's more,

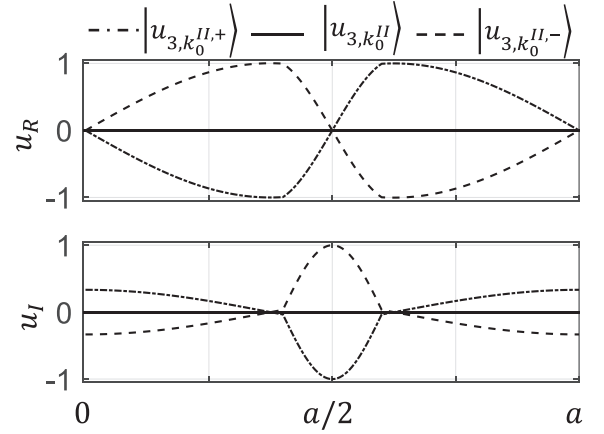


FIG. 2. Distribution of the field prior to $(k_0^{II,-})$ and subsequent to $(k_0^{II,+})$ the singularity, where u_R and u_I denote the real and imaginary components, respectively, of the normalized periodic part of the magnetic field within a single unit cell.

locating the singularity from a scattering perspective proves challenging, as computing the scattering of a half-infinite 2D-PhC is a complex task. In the following section, we will introduce the EPWE to overcome computational challenges associated with the scattering of a half-infinite 2D-PhC and elucidate the connection between scattering singularities and the directional Zak phase in 2D-PhC.

A. Method: Expanded plane wave expansion method

Considering a nonmagnetic medium and taking transverse-magnetic (TM) polarization (E^z) as an example, the governing equation for the master function of Maxwell's equations is expressed as

$$\frac{1}{\varepsilon(\mathbf{r})} \nabla \times \nabla \times E^z(\mathbf{r}, \omega) = k_0^2 E^z(\mathbf{r}, \omega), \quad (3)$$

where $k_0 = \omega/c$. We expand E^z and $\varepsilon(\mathbf{r})$ in Fourier space as $E^z(\mathbf{r}) = \sum_{\mathbf{G}} e^{i(\mathbf{k}+\mathbf{G})\cdot\mathbf{r}} E_{\mathbf{k},\mathbf{G}}^z$ and $\varepsilon(\mathbf{r}) = \sum_{\mathbf{G}} e^{i\mathbf{G}\cdot\mathbf{r}} \varepsilon_{\mathbf{G}}$, where \mathbf{G} is the reciprocal lattice vector. Equation (3) is then rewritten in Fourier space as

$$\sum_{\mathbf{G}'} \varepsilon_{\mathbf{G}-\mathbf{G}'}^{-1} (\mathbf{k} + \mathbf{G}) \cdot (\mathbf{k} + \mathbf{G}') E_{\mathbf{k},\mathbf{G}'}^z = k_0^2 \sum_{\mathbf{G}'} E_{\mathbf{k},\mathbf{G}'}^z. \quad (4)$$

Equation (4) represents an eigenfunction, allowing the determination of the band structure and eigenfield of a 2D-PhC. However, it remains insufficient for solving the scattering problem due to challenges in defining an "interface" and an input source. To address this, we rewrite Eq. (4) as

$$\begin{bmatrix} 0 \\ \varepsilon_{\mathbf{G}-\mathbf{G}'}^{-1} [k_0^2 - \varepsilon_{\mathbf{G}'-\mathbf{G}'}^{-1} (\mathbf{G}'' + k_y \hat{\mathbf{y}}) \cdot (\mathbf{G}' + k_y \hat{\mathbf{y}})] \end{bmatrix} - \varepsilon_{\mathbf{G}-\mathbf{G}'}^{-1} \begin{bmatrix} \hat{\mathbf{I}} \\ \varepsilon_{\mathbf{G}'-\mathbf{G}'}^{-1} (\mathbf{G}'_x + \mathbf{G}'_x) \end{bmatrix} \begin{bmatrix} E_{\mathbf{G}'} \\ k_x E_{\mathbf{G}'} \end{bmatrix} = k_x \begin{bmatrix} E_{\mathbf{G}'} \\ k_x E_{\mathbf{G}'} \end{bmatrix}, \quad (5)$$

where $\mathbf{k} = k_x \hat{\mathbf{x}} + k_y \hat{\mathbf{y}}$. In this equation, k_y and k_0 are fixed, and the determined parameter is k_x . This equation is suitable when the interface lies along the y direction [see Fig. 3(a)]. A similar equation can be derived for scenarios where the interface is along the x direction, in which case k_x and k_0 are fixed, and

the determined parameter is k_y . This equation is suitable for addressing inclined incidences from a homogeneous medium (region I) to a half-infinite 2D-PhC (region II), as illustrated in Fig. 3(a). By applying boundary condition, the relationship between the E^z fields in region I and region II can be

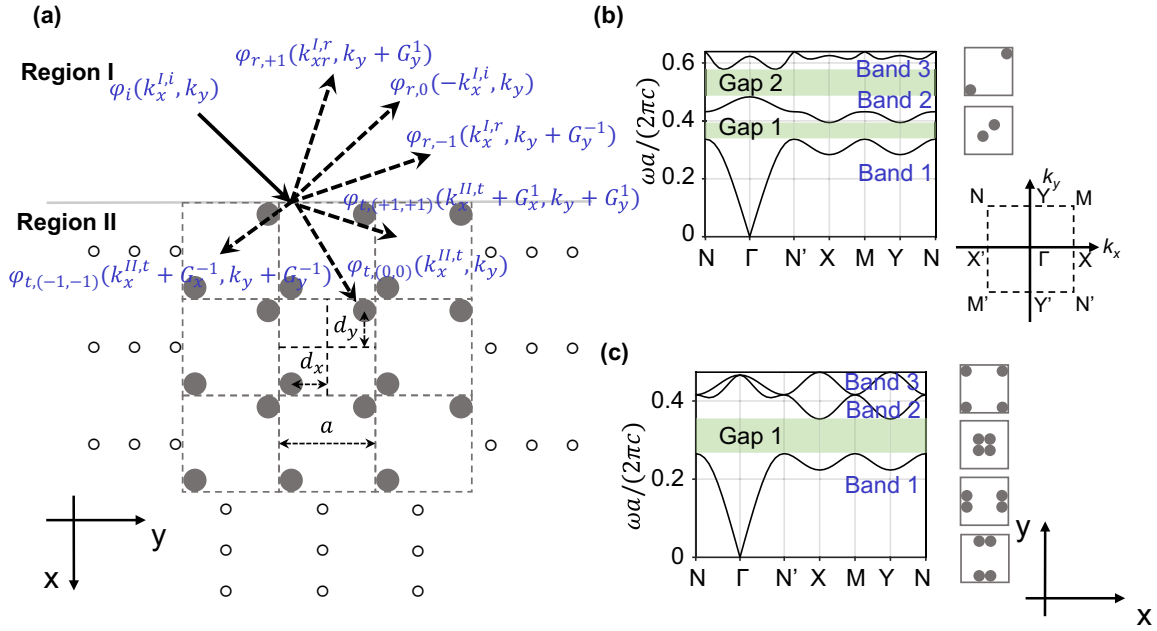


FIG. 3. (a) Schematic representation of the structure and EPWE method; (b) Band structure of the two-rods model, along with the first Brillouin zone, where the two unit cells on the right exhibit the same band structure in the left; (c) Band structure of the four-rods model, where the four unit cells in the right share the same band structure in the left.

established as follows:

$$\begin{aligned} & \begin{bmatrix} -\langle x_0 y | E_m^{z,I} \rangle & \langle x_0 y | E_m^{z,II} \rangle \\ -\langle x_0 y | \partial_x | E_m^{z,I} \rangle & \langle x_0 y | \partial_x | E_m^{z,II} \rangle \end{bmatrix} \begin{bmatrix} \langle E_m^{z,I} | \hat{\mathbf{r}} | E_0^{z,I} \rangle \\ \langle E_m^{z,II} | \hat{\mathbf{t}} | E_0^{z,I} \rangle \end{bmatrix} \\ & = \begin{bmatrix} \langle x_0 y | E_0^I \rangle \\ \langle x_0 y | \partial_x | E_0^I \rangle \end{bmatrix}, \end{aligned} \quad (6)$$

where $\hat{\mathbf{r}}$ and $\hat{\mathbf{t}}$ are the reflection and transmission operators. $E_m^{I(II)}$ represents the m th reflected (transmitted) mode in region I (II), and E_0^I is the incident field.

In this equation, E_m^{II} can be solved by Eq. (5). Regarding the eigenvectors in region I with homogeneous media, they are represented by plane waves and solely depend on G_y . Specifically, assuming the input wave vector is $\mathbf{k}_i = [k_x^{I,i}, k_y]$, according to Bloch theory, the reflection wave vector is $\mathbf{k}_r = [-\sqrt{k_0^2 - (k_y + G_y)^2}, k_y + G_y]$, and the transmission wave vector is $\mathbf{k}_t = (k_x^{II,t} + G_x, k_y + G_y)$, where $k_x^{II,t}$ also can be solved by using Eq. (5). Therefore, if we have knowledge of the structure function $\varepsilon(\mathbf{r})$, the incident wave vector \mathbf{k}_i , and the frequency of incident plane wave ω , we can solve the interface problem between a half-infinite homogeneous media and a half-infinite 2D-PhC by utilizing Eqs. (5) and (6). We should note that, the reflective spectrum, calculated using EPWE, is projected in a specific direction. For instance, when the interface is perpendicular to the x direction, as shown in Fig. 3(a), we exclusively consider specific modes in which the parallel wave vector component k_y matches that of the incident light wave. This requirement stems from the conservation of k_y on both sides of the interface. As a result, the reflective spectrum can be denoted as $R_x(k_y)$ or $R_y(k_x)$, signifying the reflectivity from the interface is perpendicular to the x direction or y direction, respectively.

B. Results

In this subsection, we will investigate two cases to illustrate topological singularities in 2D-PhC using EPWE. In the first case, depicted in Fig. 3(b), the two-rods model lacking C_4 and $M_{x(y)}$ symmetries exhibits two clearly defined lowest bands without degeneracy. This characteristic makes it an ideal model for investigating the topological phase transition between these two lowest bands. In the second case, our focus is on examining the topological phase of the first band in different directions within a four-rods model, as shown in Fig. 3(c). In both cases, the rods with a radius of $r = 0.12a$ are composed of $\varepsilon = 12$ material and are situated in the air. Additionally, TM polarization is considered. It is worth noting that the right two unit cells in Fig. 3(b) and the right four unit cells in Fig. 3(c) have the same band structures, respectively, because only the centering point of the unit cells is changing. For an infinite bulk crystal where the interface is neglected, their eigenfrequencies are the same.

Before presenting the results, we should highlight the calculation of directional Zak phase in 2D-PhC [15,23]. While akin to the computation of 1D Zak phase in Sec. II, it involves the integration of the Berry connection in two directions

$$\phi_{l,n}^{\text{Zak}} = \int_{\text{FBZ}} dk_x dk_y i \langle u_{n,k} | \partial_{k_l} u_{n,k} \rangle, \quad l = x, y. \quad (7)$$

We can alternatively utilize the Wilson loop to obtain the 2D Zak phase. For instance, selecting a fixed k_y and the Zak phase in the x direction at this fixed k_y is given by

$$\phi_{x,n}^{\text{Zak}}(k_y) = \sum_{j \in \text{FBZ}} -\text{Im} \ln [\langle u_{n,k_x,j} | u_{n,k_x,j+1} \rangle]. \quad (8)$$

Additionally, directional polarization can be employed to ascertain topology, denoted as $\mathbf{P}_n = [P_{x,n}, P_{y,n}] = [\phi_{x,n}^{\text{Zak}},$

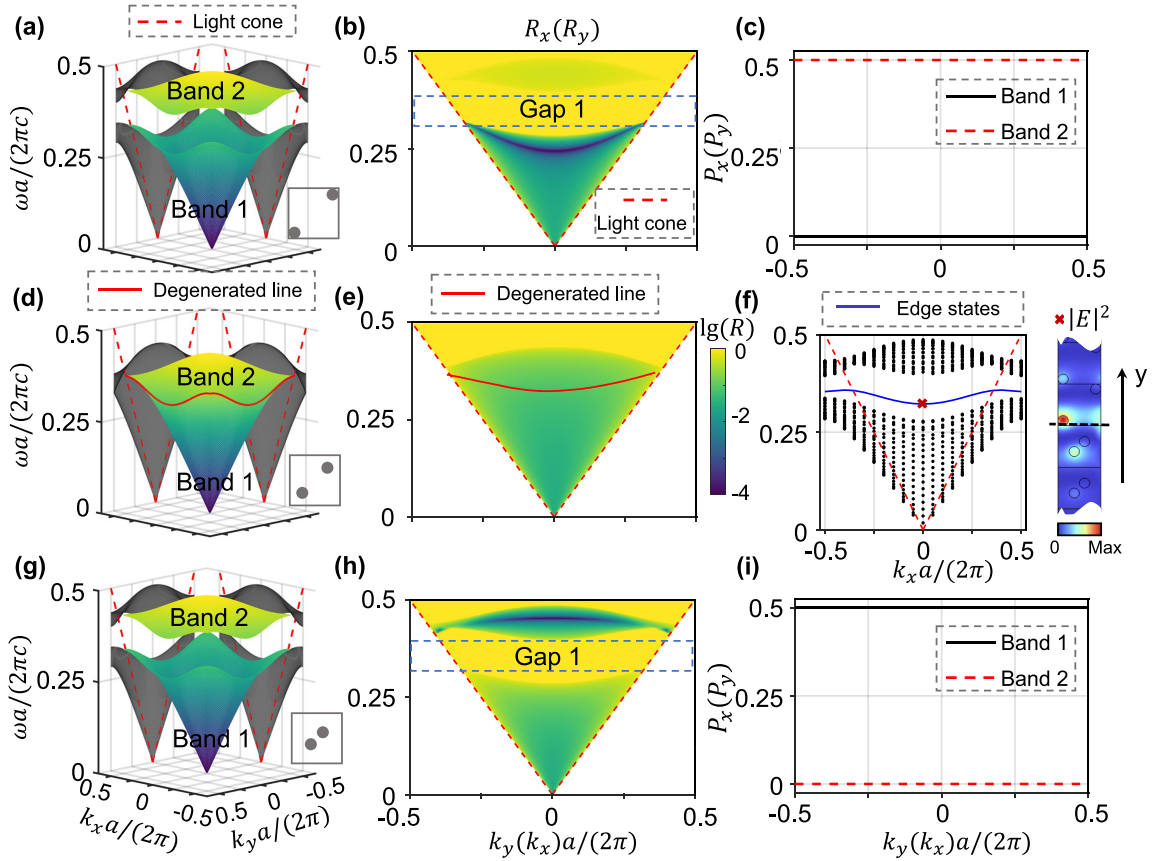


FIG. 4. Singularity-induced topological phase transition in 2D-PhC. (a)–(c) Band structure in three dimensional and the projected band structure in the x (y) direction, reflective spectrum $R_x(k_y)$ or $R_y(k_x)$, and the directional polarization of the two lowest bands, respectively, where the parameters are $r = 0.12a$, $\varepsilon = 12$, $d_x = d_y = 0.12a$; (d), (e) The same as (a), (b) but $d_x = d_y = 0.25a$; (g)–(i): The same as (a)–(c) but $d_x = d_y = 0.38a$; (f): The band structure that combines ten layers of the model in (a) with ten layers of the model in (g), along with the $|E|^2$ distribution, where the band of edge states is marked with blue line.

$\phi_{y,n}^{\text{Zak}}]/(2\pi)$. Consequently, we can correlate the directional polarization $P_x(k_y)$ or $P_y(k_x)$ to the reflective spectrum $R_x(k_y)$ or $R_y(k_x)$, respectively.

1. Singularity-Induced topological phase transition between two bands

Similar to the topological phase transition discussed in Sec. II, we construct a square lattice to break C_4 and $M_{x(y)}$ symmetries, then by varying the distance between the rods and the cell center, we investigate the entire topological phase transition in the lowest two bands. We maintain equal distances between the two rods and the cell center $d_x = d_y$, so the band structure and band topology remain identical in both x and y directions. Therefore, the x label in Figs. 4(b), 4(e), 4(h), 4(c), and 4(i) can represent either k_x or k_y . Accordingly, the reflective spectrum in Figs. 4(b), 4(e), and 4(h) can indicate the corresponding $R_y(k_x)$ or $R_x(k_y)$, respectively. Similarly, the polarization in Figs. 4(c) and 4(i) can represent either $P_y(k_x)$ or $P_x(k_y)$, respectively.

In the case presented in Figs. 4(a)–4(c), where the rods are positioned far away from the cell center ($d_x = d_y = 0.38a$), the band topology in Fig. 4(c) reveals that $\mathbf{P}_1 = [0.5, 0.5]$ and $\mathbf{P}_2 = [0, 0]$. The topological scattering singularity in this scenario is particularly intriguing, with the zero-reflection

phenomenon no longer manifesting as a point but as a line in the first band, as shown in Fig. 4(b) with deep blue lines. This observation aligns with the directional polarization in Fig. 4(c): for any fixed k_x or k_y , if $P_{1,x}(k_y) = 0.5$ or $P_{1,y}(k_x) = 0.5$, the projected reflective spectrum $R_x(k_y, \omega)$ or $R_y(k_x, \omega)$ exhibits a zero-reflection line.

By varying d_x and d_y , we can induce a topological phase transition through a gap-close-reopen process. In Figs. 4(d) and 4(e), the first gap closes when $d_x = d_y = 0.25a$. Further decreasing d_x and d_y to $0.12a$ reopens the first gap, as shown in Fig. 4(g), and the topology of the lowest bands becomes opposite to the first case. In this scenario, there is no zero-reflection singularity in the first band of the projected reflective spectrum, and the zero-reflection singularity is observed in the second band. It's observed that the second band may overlap when projected to one direction, especially near the band edge, but this does not affect our conclusions.

Additionally, combining the two types of 2D-PhC in Figs. 4(a) and 4(g) to verify the topology, the band structure and field distribution of edge states are illustrated in Fig. 4(f). Notably, the band of edge states in the first gap is clearly discernible, along with the presence of a localized edge state with $k_x = 0$.

Lastly, the robustness of the singularity is demonstrated through the use of this model in the Appendix. It is shown

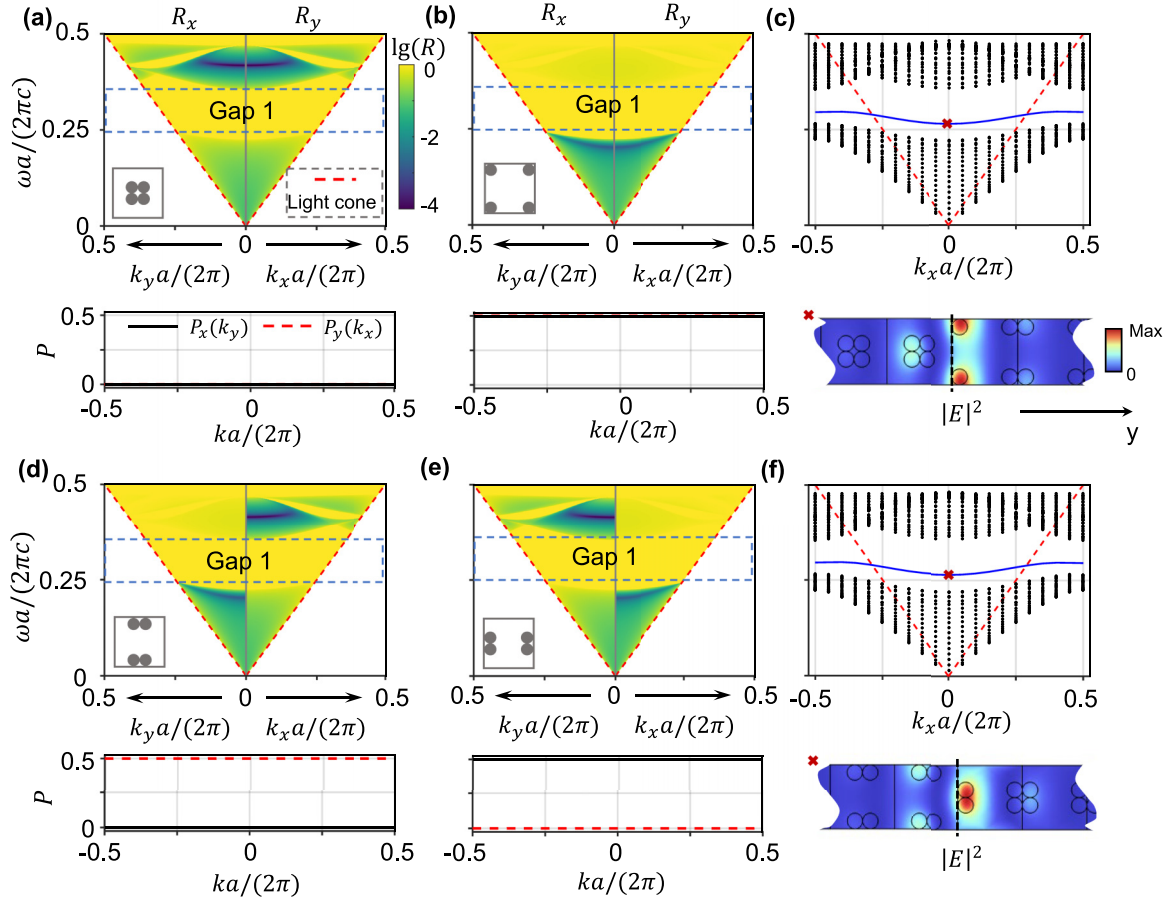


FIG. 5. Singularity behavior in directional Zak phase. (a) Top: reflective spectrum $R_x(k_y)$ along $k_y a/(2\pi)$ from 0 to 0.5 (left) and $R_y(k_x)$ along $k_x a/(2\pi)$ from 0 to 0.5 (right). Bottom: directional polarization of the first band in different directions, with parameters $d_x = d_y = 0.12a$; (b) the same as (a) but $d_x = d_y = 0.38a$; (c) Band structure combining ten layers of the model in (a) with ten layers of the model in (b), along with the $|E|^2$ distribution. (d) the same as (a) but $d_x = 0.12a$, $d_y = 0.38a$; (e) the same as (a) but $d_x = 0.38a$, $d_y = 0.12a$; (f) Band structure combining ten layers of the model in (d) with ten layers of the model in (e), along with the $|E|^2$ distribution.

that the singularity persists for a topologically nontrivial band, even when a weak random disorder is introduced into PhCs.

2. Singularity behavior in directional Zak phase

In this subsection, we delve into the nuanced intricacies of the topological singularity's behavior within the directional Zak phase, offering a comprehensive exploration of its impact on the first band in a four-rods model. By systematically varying the parameters, such as the distances between rods (d_x and d_y), we scrutinize the resulting changes in the reflective spectrum's symmetry and the emergence of zero-reflection lines.

In cases where d_x equals d_y , i.e., $d_x = d_y = 0.12a$ or $d_x = d_y = 0.38a$, we plot $R_y(k_x)$ and $R_x(k_y)$ along different directions, as portrayed in Figs. 5(a) and 5(b). The reflective spectrum exhibits notable symmetrical characteristics along $k_x(k_y) = 0$, culminating in a reflective symmetry axis. Our analysis discerns the absence of a zero-reflection line in the trivial first band, contrasting sharply with the discernible zero-reflection line in the nontrivial first band. The nuanced symmetry deviations are further underscored by the pronounced presence of edge states in the combined models of these two distinct photonic crystals.

The exploration extends to scenarios where $d_x \neq d_y$, i.e., $d_x = 0.12a$, $d_y = 0.38a$ or $d_x = 0.38a$, $d_y = 0.12a$, as exemplified in Figs. 5(d) and 5(e). In such instances, the once symmetrical reflective spectrum along $k_x(k_y) = 0$ undergoes a transformative shift, eliminating the reflective symmetry axis. The nontrivial direction of the first band, where $P_x(P_y) \neq 0$, distinctly manifests a discernible zero-reflection line in the $k_y(k_x)$ direction. In contrast, the trivial direction exhibits the absence of such a line. This observation is further validated by the unequivocal presence of edge states in the combined model of the two diverse photonic crystals.

From our two examples, it is important to note that even if two or more cells have the same band structure, their reflective spectra may differ fundamentally. Our work provides a scattering view to reveal the deep topology beyond the band structure.

IV. CONCLUSIONS

In summary, this study has unveiled an approach for discerning the topology of isolated bands in classical wave systems, both in one and two dimensions, leveraging the concept of a topological singularity characterized by a

zero-reflection point or line. Our investigations in the two-dimensional domain revealed that the dynamic movement of this topological singularity induces significant topological phase transitions. The existence of topological singularities in diverse directions imparts distinct topological properties along those specific axes. Our contributions extend beyond traditional tight-binding models, as demonstrated by the designed models showcasing topological phase transitions in two-dimensional photonic crystals. These findings underscore the profound impact of the topological singularity on reflective phenomena, shedding light on the intricate interplay between symmetry, zero-reflection lines, and band topology. The proposed methodology not only enriches our fundamental understanding of topological phases but also opens avenues for practical applications in the design and engineering of topological devices. As an illustration, even if a system possesses a directional band gap, rendering topological edge states unobservable directly, the reflection spectrum can still serve as an indicator of whether the band is topological. As future work, we anticipate further exploration of topological aspects in diverse topological insulators, such as the photonic Chern insulator. Our prior research has revealed that in one-dimensional systems with synthetic dimensions, the scattering singularity of the photonic Chern insulator remains a point. It would be both intriguing and essential to extend our methodologies to analyze the scattering singularities in actual two-dimensional photonic Chern insulators composed of anisotropic materials. Moreover, delving into non-Abelian topology, particularly in cases where band overlap is complex, and scrutinizing non-Hermitian systems, also offer compelling directions for future research.

The code used to calculate the band and reflective spectrum is available at [39].

ACKNOWLEDGMENTS

This work is supported by the National High Technology Research and Development Program of China (17-H863-04-ZT-001-035-01); the National Key Research and Development Program of China (2016YFA0301103, 2018YFA0306201); and the National Natural Science Foundation of China (12174073). G.H. acknowledges the Nanyang Assistant Professorship Start-up Grant and Ministry of Education (Singapore) under AcRF TIER1 (RG61/23). L.X. acknowledges the insightful discussions with Ms. Xiaoyuan He.

The authors declare no conflicts of interest.

APPENDIX: ROBUSTNESS OF SINGULARITY

In discussing the robustness of the singularity, it is crucial to acknowledge that the 2D scattering computations delineated in our work rely on the plane wave expansion method. This method is intrinsically appropriate for periodic boundary conditions and, therefore, is not applicable to disordered systems. To probe the robustness of the singularity amidst disorder, we adopted a numerical strategy utilizing a finite photonic crystal structure comprised of five unit cells.

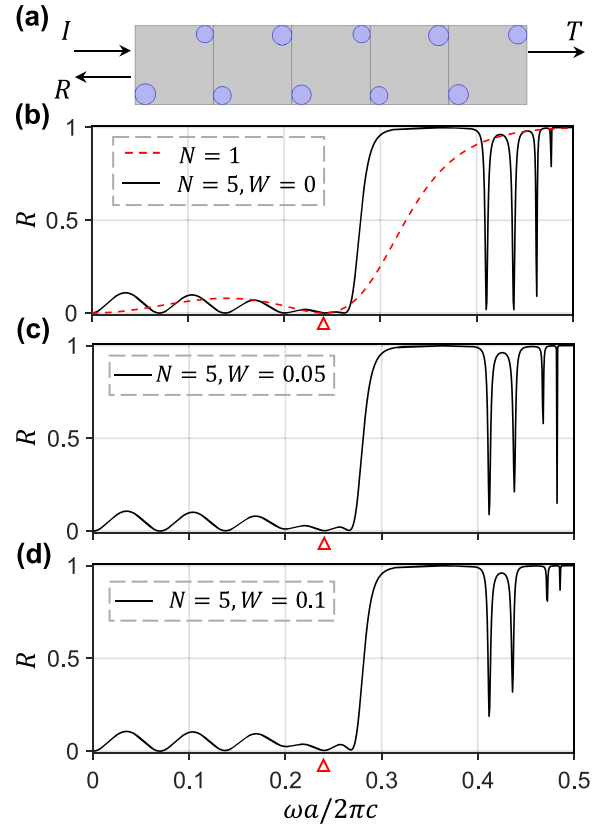


FIG. 6. Robustness of singularity. (a) Schematic of a finite periodic 2D photonic crystal with five unit cells, where periodic boundary conditions are applied to the top and bottom boundaries. The radius of each rod is given by $r = r_0 \gamma W$, where $\gamma \in [-1, 1]$ is a random variable, W is the disorder strength (in this figure, $W = 0.1$), and r_0 is the initial radius $0.12a$. (b) Reflectivity of a single unit cell (red dashed line) and five unit cells (black solid line, $W = 0$). The red triangle marks the resonance frequency (i.e., singularity) of a single unit cell. (c) Reflectivity of five disordered unit cells with $W = 0.05$. (d) Reflectivity of five disordered unit cells with $W = 0.1$.

Drawing upon the findings of [35], for a finite PhC comprising N unit cells, the transmittance of the finite PhC is given by

$$T^{-1} = 1 + \frac{\sin^2 N\phi}{\sin^2 \phi} \left(\frac{1}{|t_1|^2} - 1 \right). \quad (\text{A1})$$

From Eq. (A1), it is evident that within each band, there are $N - 1$ peaks, which originate from Bragg reflections at frequencies that satisfy $N\phi = m\pi$, where $m = 1, 2, \dots, N - 1$. Additionally, another resonance peak of the finite periodic system appears at frequencies where the unit-cell transmittance is $|t_1|^2 = 1$. In essence, if a resonant frequency of a single unit cell (i.e., a singularity) exists within the band, the system will exhibit N resonance peaks. Conversely, in the absence of such a singularity, there will be $N - 1$ resonance peaks.

For instance, consider the unit cell depicted in Fig. 4(a), and a finite PhC with five cells ($N = 5$) as shown in Fig. 6(a). Initially, for the perfect PhC devoid of disorder, we observe that the nontrivial first band has five resonance peaks, and

the trivial second band has four resonance peaks in Fig. 6(b). Furthermore, upon plotting the reflectivity of a single unit cell, we find that the additional resonance peak in the first band coincides with the resonance of a single unit cell.

Additionally, we introduce a weak random disorder to the radius of the dielectric rods, denoted as $r = r_0\gamma W$, where W represents the disorder strength and γ is a random number within the range $[-1, 1]$. In Figs. 6(c) and 6(d), we assign values of $W = 0.05$ and $W = 0.1$, respectively. It is observed

that there are five distinct peaks in the first nontrivial band and four peaks in the second trivial band for both cases of random disorder. It is noteworthy that the disorder strength $W = 0.1$ falls within the fabrication tolerances [40]. This observation underscores that the topologically nontrivial nature of the band ensures the persistence of the singularity, even in the presence of weak disorder. Consequently, the robustness of the singularity serves as a significant indicator of the topological integrity of the system.

-
- [1] X.-L. Qi and S.-C. Zhang, Topological insulators and superconductors, *Rev. Mod. Phys.* **83**, 1057 (2011).
- [2] M. Z. Hasan and C. L. Kane, *Colloquium: Topological insulators*, *Rev. Mod. Phys.* **82**, 3045 (2010).
- [3] A. Bansil, H. Lin, and T. Das, *Colloquium: Topological band theory*, *Rev. Mod. Phys.* **88**, 021004 (2016).
- [4] C.-K. Chiu, J. C. Y. Teo, A. P. Schnyder, and S. Ryu, Classification of topological quantum matter with symmetries, *Rev. Mod. Phys.* **88**, 035005 (2016).
- [5] T. Ozawa, H. M. Price, A. Amo, N. Goldman, M. Hafezi, L. Lu, M. C. Rechtsman, D. Schuster, J. Simon, O. Zilberberg, and I. Carusotto, Topological photonics, *Rev. Mod. Phys.* **91**, 015006 (2019).
- [6] M. S. Rider, S. J. Palmer, S. R. Poojari, X. Xiao, P. Arroyo Huidobro, and V. Giannini, A perspective on topological nanophotonics: Current status and future challenges, *J. Appl. Phys.* **125**, 120901 (2019).
- [7] L. Lu, J. D. Joannopoulos, and M. Soljačić, Topological photonics, *Nat. Photon.* **8**, 821 (2014).
- [8] A. B. Khanikaev and G. Shvets, Two-dimensional topological photonics, *Nat. Photon.* **11**, 763 (2017).
- [9] Y. Wu, C. Li, X. Hu, Y. Ao, Y. Zhao, and Q. Gong, Applications of topological photonics in integrated photonic devices, *Adv. Opt. Mater.* **5**, 1700357 (2017).
- [10] G. Hu, Q. Ou, G. Si, Y. Wu, J. Wu, Z. Dai, A. Krasnok, Y. Mator, Q. Zhang, Q. Bao *et al.*, Topological polaritons and photonic magic angles in twisted α -MoO₃ bilayers, *Nature (London)* **582**, 209 (2020).
- [11] L. Xiong, Y. Zhang, and X. Jiang, Resonance and topological singularity near and beyond zero frequency for waves: model, theory, and effects, *Photonics Res.* **9**, 2024 (2021).
- [12] M. Kim, Z. Jacob, and J. Rho, Recent advances in 2D, 3D and higher-order topological photonics, *Light: Sci. Appl.* **9**, 130 (2020).
- [13] B. Xie, H.-X. Wang, X. Zhang, P. Zhan, J.-H. Jiang, M. Lu, and Y. Chen, Higher-order band topology, *Nat. Rev. Phys.* **3**, 520 (2021).
- [14] Y. Liu, S. Leung, F.-F. Li, Z.-K. Lin, X. Tao, Y. Poo, and J.-H. Jiang, Bulk–disclination correspondence in topological crystalline insulators, *Nature (London)* **589**, 381 (2021).
- [15] B.-Y. Xie, H.-F. Wang, H.-X. Wang, X.-Y. Zhu, J.-H. Jiang, M.-H. Lu, and Y.-F. Chen, Second-order photonic topological insulator with corner states, *Phys. Rev. B* **98**, 205147 (2018).
- [16] B.-Y. Xie, G.-X. Su, H.-F. Wang, H. Su, X.-P. Shen, P. Zhan, M.-H. Lu, Z.-L. Wang, and Y.-F. Chen, Visualization of higher-order topological insulating phases in two-dimensional dielectric photonic crystals, *Phys. Rev. Lett.* **122**, 233903 (2019).
- [17] L. Xiong, Y. Liu, Y. Zhang, Y. Zheng, and X. Jiang, Topological properties of a two-dimensional photonic square lattice without C_4 and $M_{x(y)}$ symmetries, *ACS Photonics* **9**, 2448 (2022).
- [18] W. A. Benalcazar, B. A. Bernevig, and T. L. Hughes, Quantized electric multipole insulators, *Science* **357**, 61 (2017).
- [19] L. He, Z. Addison, E. J. Mele, and B. Zhen, Quadrupole topological photonic crystals, *Nat. Commun.* **11**, 1 (2020).
- [20] W. A. Benalcazar, B. A. Bernevig, and T. L. Hughes, Electric multipole moments, topological multipole moment pumping, and chiral hinge states in crystalline insulators, *Phys. Rev. B* **96**, 245115 (2017).
- [21] Wikipedia, <https://en.wikipedia.org/wiki/Topology>
- [22] J. Zak, Berry's phase for energy bands in solids, *Phys. Rev. Lett.* **62**, 2747 (1989).
- [23] F. Liu and K. Wakabayashi, Novel topological phase with a zero Berry curvature, *Phys. Rev. Lett.* **118**, 076803 (2017).
- [24] R. Zhao, G.-D. Xie, M. L. N. Chen, Z. Lan, Z. Huang, and W. E. I. Sha, First-principle calculation of Chern number in gyrotropic photonic crystals, *Opt. Express* **28**, 4638 (2020).
- [25] X. Xi, K.-P. Ye, and R.-X. Wu, Topological photonic crystal of large valley Chern numbers, *Photonics Res.* **8**, B1 (2020).
- [26] Z. Wang, Y. D. Chong, J. D. Joannopoulos, and M. Soljačić, Reflection-free one-way edge modes in a gyromagnetic photonic crystal, *Phys. Rev. Lett.* **100**, 013905 (2008).
- [27] J. K. Asbóth, L. Oroszlány, and A. Pályi, A short course on topological insulators, *Lect. Notes Phys.* **919**, 23 (2016).
- [28] Q. Li and X. Jiang, Singularity induced topological transition of different dimensions in one synthetic photonic system, *Opt. Commun.* **440**, 32 (2019).
- [29] J. D. Joannopoulos, S. G. Johnson, J. N. Winn, and R. D. Meade, *Photonic Crystals: Molding the Flow of Light* (Princeton University Press, Princeton, 2011).
- [30] M. Xiao, Z. Q. Zhang, and C. T. Chan, Surface impedance and bulk band geometric phases in one-dimensional systems, *Phys. Rev. X* **4**, 021017 (2014).
- [31] Y.-C. Hsue, A. J. Freeman, and B.-Y. Gu, Extended plane-wave expansion method in three-dimensional anisotropic photonic crystals, *Phys. Rev. B* **72**, 195118 (2005).
- [32] Y.-C. Hsue and T.-J. Yang, Applying a modified plane-wave expansion method to the calculations of transmittivity and reflectivity of a semi-infinite photonic crystal, *Phys. Rev. E* **70**, 016706 (2004).
- [33] Y. Liu, L. Xiong, and X. Jiang, The evolution of topological singularities between real-and complex-frequency domains and the engineering of photonic bands for Hermitian and non-Hermitian photonic crystals, *New J. Phys.* **24**, 123042 (2022).

- [34] Q. Li, Y. Zhang, and X. Jiang, Two classes of singularities and novel topology in a specially designed synthetic photonic crystals, *Opt. Express* **27**, 4956 (2019).
- [35] P. A. Kalozoumis, G. Theocharis, V. Achilleos, S. Félix, O. Richoux, and V. Pagneux, Finite-size effects on topological interface states in one-dimensional scattering systems, *Phys. Rev. A* **98**, 023838 (2018).
- [36] L. Zhang, Y. Zhang, X. Chen, X. Liu, L. Zhang, and H. Chen, Study on the tunneling mode in a sub-wavelength open-cavity resonator consisting of single negative materials, *IEEE Trans. Antennas Propag.* **62**, 504 (2013).
- [37] X. Shi, C. Xue, H. Jiang, and H. Chen, Topological description for gaps of one-dimensional symmetric all-dielectric photonic crystals, *Opt. Express* **24**, 18580 (2016).
- [38] It's essential to note that $[\langle u_{n,k_j} | u_{n,k_{j+1}} \rangle]$ should be normalized in all of our cases.
- [39] <https://github.com/kabume/Peacock.jl>
- [40] Y. Ma, Y. Xia, J. Liu, S. Zhang, J. Shao, B.-R. Lu, and Y. Chen, Processing study of SU-8 pillar profiles with high aspect ratio by electron-beam lithography, *Microelectron. Eng.* **149**, 141 (2016).